2 Simulation of detector and physics performance

2.1 Introduction

This chapter presents the software tools used throughout this document to evaluate in a consistent way the detailed performance of the various detector systems, both individually (see Chapters 3 to 6) and combined (see Chapters 7 to 13), as well as the corresponding physics performance over a wide variety of different topics (see Chapters 14 to 21).

The requirements from these two aspects of the work (detector performance and physics performance) are sometimes conflicting:

- the detector simulation (Inner Detector, LAr and Tile Calorimeters and Muon System) and combined-performance (*b*-tagging, electrons / photons, jets / $E_{\mathrm{T}}^{\mathrm{miss}}$ / τ-leptons, muons and trigger) working groups have, in most cases, been the promoters of detailed simulations using the GEANT package (version 3.21) [2-1], as described in Section 2.2. These simulations have to be performed in an environment containing many interactions per beam-crossing (in the case of the Inner Detector and calorimeters) and high rates of background noise from low-energy neutrons (in the case of the Muon System), as described in Section 2.3. These groups have also performed detailed studies requiring the full reconstruction of samples of individual particles or of complete physics events, as described in Section 2.4;
- in contrast, the physics-simulation working groups (Higgs bosons, supersymmetry, B-physics and top physics) have concentrated in most cases on fast simulation of high-statistics signal and background samples of complete physics events, as described in Section 2.5. Whenever deemed necessary, *e.g.* when studying invariant masses of reconstructed final-state objects originating from the decay of a narrow resonance, results from full simulation and reconstruction have been used to improve, refine and enrich the fast-simulation program.

The software tools and their technical and performance aspects described below have been developed over the past decade or so, but are now quite complete, from the tools devoted to accurate Monte Carlo generation of complex physics processes, to interactive graphics tools devoted to dynamically display and modify the results of the reconstruction programs, and finally to the tools devoted to interactive physics analysis of very large datasets. They meet in many areas the requirements needed for the final ATLAS software and will have to be maintained active, as a reference, over the next years, while the OO / C++ software for the experiment is designed and produced.

2.2 Full simulation of ATLAS response

2.2.1 General considerations

The complexity of the physics events to be analysed at the LHC and the diversity of the detectors to be integrated into ATLAS make it an absolute necessity to provide an accurate detector simulation program, with which the detector and physics performance can be evaluated in de-

tail. Such a program must be extremely flexible in all its components, in order to meet the wide variety of requirements, which appear throughout the development phase of the experiment. These requirements are very stringent, especially for the detector geometry modules, which must be very powerful and versatile, in order to describe the very complicated experimental setup foreseen for ATLAS, while at the same time maintaining the possibility of changing or replacing parts of the detector in a simple and reproducible way.

The second problem, which the detector simulation program must solve as efficiently and as realistically as possible, is how to reproduce faithfully the harsh experimental conditions to be encountered during operation at the LHC. As is well understood after almost a decade of simulation work, these conditions are the source of phenomena which have in many ways shaped the detector design (event pile-up, radiation background, detector occupancy and background noise). Given the huge complexity of the detector geometry which the simulation program must deal with, one simply cannot afford to simulate complete bunch crossings (which involve 23 inelastic interactions on average at the LHC design luminosity) for different values of the instantaneous luminosity. One must rather find a way to simulate single events and then to add them up (while respecting the time structure of the event) in a sufficient number to reproduce a beam crossing. The same is true for the noise in the detector, which in many cases depends crucially on the luminosity and which must be injected after the GEANT simulation has been performed. Additional requirements are imposed on the event structure passed to the reconstruction program, which must be stable and general enough to allow for an easy and robust interface between the two programs.

The ATLAS simulation program (normally referred to as DICE, Detector Integration for a Collider Experiment) has been developed continuously since 1990, as a tool to cope with the most important deadlines of the collaboration (the Letter of Intent, the Technical Proposal and the Technical Design Reports), for which ever more detailed results concerning the detector performance expected at the LHC have been reported.

The first version of DICE was optimised for conceptual layout studies with all possible options for the various subdetectors ready to be activated and to be assembled into one of the proposed layouts; in this case, the geometrical description was a relatively simple one, with none of the detectors as accurately represented as they are today, in order to save CPU time and to permit different configurations to be studied in parallel.

In the second version of DICE, the geometrical representation of all subdetectors was improved and specialised to include all of the details envisaged as relevant at a certain time. Nevertheless, where two or more options were available for a subdetector, it was still possible to replace complete parts of that particular subdetector.

The third (and current) version of DICE contains an even more specialised version of the geometry representation, where only small adjustments are possible, to take into account detector layout modifications, and to deal with the increased complexity of the geometry description. Utility libraries for building the geometry in a standardised way have been provided, together with a macro-based language which gives definite advantages in terms of description uniformity and bank manipulation.

2.2.2 Infrastructure

The ATLAS simulation program can be logically divided into three separate modules:

- event generation;
- detector simulation;
- digitisation.

These three parts communicate through a set of ZEBRA banks and can be run separately or in sequence. The framework for the simulation program is provided by a package called SLUG (Simulation for LHC Using GEANT). SLUG provides the basic infrastructure for handling ZEBRA banks. It also provides a set of facilities for dealing with event generation, detector geometry and simulation, event merging for pile-up studies, together with stubs for user-defined routines to gain access to every step in the simulation process and tools for managing histograms and n-tuples. The program flow is controlled via an extensive set of pre-defined command procedures, which the user can control and execute through FFREAD datacards. Although some interactive functionality was initially provided, the program has normally been run in batch mode for production purposes. An interactive facility (ATLSIM), built essentially around the same basic components, has been provided and used for development work using the simulation and reconstruction software.

The DICE package contains general-purpose routines, which control the simulation flow, together with detector geometry modules, digitisation routines, and dedicated routines to model the detector response better than GEANT wherever needed (see Section 2.2.3).

2.2.3 GEANT model and parameters

As stated above, the GEANT package has been used to simulate in detail the detector characteristics and performance: several versions (3.14, 3.15, 3.21) have been run in production during the evolution of the detector simulation software. Version 3.21 is the one best suited for describing some of the very complex aspects of the detector geometry (*e.g.* the Accordion calorimeter), while still providing a reasonable performance in terms of accuracy of the simulation and of CPU time needed to track particles through the complete detector. In addition to describing the detector geometry and tracking particles through it, the GEANT framework is used to describe the materials constituting the detector, to visualise the detector components, and to simulate and record the response of the sensitive elements of the various systems.

When simulating a very complex detector such as ATLAS, the simulation software has to take into account as large a number of physics processes as possible, covering the broadest possible range of energies. Ideally, the program should be able to simulate physics processes with energies as low as 10 eV (*e.g.* ionisation potential in the active gas of various detectors) and as high as a few TeV (*e.g.* catastrophic energy losses of muons traversing the calorimeters). The most challenging task in terms of consumption of CPU time is an accurate simulation of showers in the calorimeters. The critical areas of the GEANT model for each specific detector system are:

- the tracking detectors require ideally a detailed and microscopic simulation of all processes which could affect the track reconstruction efficiency and the momentum measurement. None of the current implementations of *dE/dx* processes nor even of hadronic processes is adequate for the specific requirements of the Inner Detector. In particular, the transition radiation process is not implemented in GEANT and, to understand the electron identification ability of the TRT, careful calculations of the energy deposited by ioni-

sation and transition radiation in the straws have been developed. The ionisation energy is calculated using the Photon Absorption Ionisation (PAI) model, whilst transition radiation photons are generated with the correct energy spectrum (from test beam results) and tracked through the experimental setup by GEANT. All transport cuts have been set at 100 keV for the Inner Detector, whereas the cut for the production of secondaries (mainly bremsstrahlung and δ-rays) has been set at 1 MeV;

- the dominant electromagnetic processes are adequately simulated by GEANT 3.21 over an energy range from 10 keV to 10 TeV. However, a very accurate simulation of electromagnetic showers in the complex geometry of the Accordion calorimeter is not affordable in terms of CPU time. The accuracy of the GEANT electromagnetic physics has been thoroughly confronted with data from test beams and has been found to be acceptable with a cut of 100 keV for electrons and photons, which represents the best compromise between accuracy and performance;
- as far as hadronic processes are concerned, both GEISHA and FLUKA (the implementation of which in GEANT 3.21 has been declared obsolete by the author) fall short of expectations, since the values for the resolution and the constant term of the Hadronic Calorimeters obtained with the simulation are quite different from the experimental results obtained from test-beam measurements. The final choice for the hadronic model was to use the GEANT interface to the CALOR package (which is in fact FLUKA for energies above a few GeV) because, although still far from an optimal fit to the data, it better reproduces the experimental results. A cut set at 1 MeV for most of the hadronic processes has been used for event production, again as a trade-off for performance.

Wherever possible, if the GEANT physics models have proven not to be adequate to the level of accuracy required for the ATLAS detector simulation program, specialised solutions have had to be adopted, as described above.

2.2.4 Geometry

The description of the ATLAS geometry in GEANT is probably the most critical issue for the detector-simulation program, since it must represent the right compromise between accuracy (which is needed to understand the most subtle systematic effects introduced by the detector layout) and performance. To simplify this procedure, a FORTRAN-based macro-language (AGE, Atlas GEant) has been used to set up detector-description banks, to implement the detector geometry, and to define HITS and DIGI structures associated with it. The advantage of this approach for the user is the possibility of having a generic interface to ZEBRA, while still maintaining a high level of flexibility.

Detector-description parameters are stored into ZEBRA banks (DETP, DETector Parameters), which can be overwritten interactively via datacards (*e.g.* for last-minute modifications), before they are used for the construction of the geometry. These banks are stored in the output file, together with the data, and may thus be used as a reference, in particular by the reconstruction program. A set of facilities (the functionality of which is greatly enhanced by parsing the AGE language into FORTRAN) is then used to build the geometry in the most general and efficient way.

All the ATLAS subdetectors have been described to a very high level of detail in DICE. Inactive material (cryostats, support structures, services, *etc*) has been given a great emphasis, and an accurate description of both its layout and material distribution has been introduced wherever possible. These inactive parts of the detector have often been shown to have a direct impact on the physics performance of the experiment and therefore have to be evaluated very carefully.

The numbers of GEANT volumes used to describe the geometry of the various ATLAS systems are shown in Table 2-1, where they can be compared to the total number of active detector elements or equivalently of independent readout channels (recipients in principle of the GEANT DIGI information, as described in Section 2.2.7), and to the total number of modules or chambers. In many systems, essentially each active cell is described explicitly, using sometimes up to ten volumes or more per cell. In contrast, details like the pixel or microstrip structure of the silicon detectors, or the cell structure of the barrel Accordion calorimeter, have not been described in the geometry itself, but only introduced afterwards at the digitisation level (see Section 2.2.7), in order to increase the flexibility and the performance of the simulation chain. Table 2-1 illustrates the complexity of the GEANT description of the ATLAS detector geometry with its 16×10^6 volumes.

Table 2-1 Number of active detector elements, number of modules or chambers, and number of GEANT volumes defined for the detailed simulation of each of the various ATLAS detector systems.

Detector system	Number of active detector elements	Number of modules or chambers	Number of GEANT volumes defined
Pixels	140 000 000	~2 200	26 000
Silicon microstrips	6 280 000	~4100	50 000
Transition radiation tracker	420 000	~240	2 260 000
LAr accordion calorimeters	170 000	48	9 960 000
LAr hadronic end-cap and forward calorimeters	9 000	134	890 000
Tile Calorimeters	10 000	192	900 000
Muon System	1 230 000	~2 000	1 850 000

The magnetic field map used by the detector simulation program has been created through a combination of specific programs (TOSCA package) to evaluate the field in the Inner Detector and the calorimeters and of analytical calculations for the Muon System. The field map is read in during the initialisation phase and stored in a ZEBRA bank, so that it can be also used by the reconstruction program. For the Inner Detector, the deviations of the solenoidal field from a constant field were considered not to be important enough in terms of performance implications (except for the impact on the momentum resolution itself, which is accounted for in most studies reported in this document) to warrant a significant change in the pattern recognition programs, and a constant field map for this part of the detector was used instead (with the exception of the study reported in Section 3.5.4).

2.2.5 Event generation

The event-generation phase is normally run separately in order to have a consistent input stream which can be used many times. Event generation facilities are implemented within SLUG by using the GENZ package, which provides a common interface between the most widely used event generators (PYTHIA, HERWIG, ISAJET) and GEANT via the standard HEPEVT common block and ZEBRA banks. A separate event generation facility, ATGEN, has also been developed to provide an analysis framework at the event level, by using the same components for booking and manipulating ZEBRA banks, so that the events produced with it can directly be read in by the standard simulation program. *Ad hoc* single-particle generators and test-beam geometries have also been developed for detector-specific studies.

The GENZ output bank can, at this point, be used to fill the GEANT KINE bank and tracking through the detector can begin. During this step, particle filter algorithms can be applied, in order not to track particles outside the geometrical acceptance of the detector or with an energy below a certain threshold, thus achieving a significant gain in CPU time. More sophisticated filter algorithms (for instance on the electromagnetic component of a jet, to see if it can fake an electron) implement a sort of 0-th level trigger, which kills those events which are not interesting for the physics channel under study.

2.2.6 Detector simulation

The detector-simulation part is the most time-consuming and critical; it can be run with different initial conditions (*e.g.* geometrical setup) on the same set of physics events in order to understand the impact of a change in the detector on the physics performance.

The particle four-vectors (stored in the GEANT KINE banks) are tracked through the various detector systems. At any time during this procedure, a snapshot of the current status can be recorded in the detector. This recording process will occur only for those parts of the detector which have been declared sensitive in the simulation program, and this is implemented first and foremost for the detector elements, where information is actually collected (*dE/dx* deposited in silicon sensors or in the active gas of straw tubes or muon chambers, light produced in scintillator tiles, *etc*). However, there exist inactive parts of the detector, *e.g.* the cryostats, for which it is of substantial interest to record the amount of ('invisible') energy deposited. This has often been used as a cross-check, *e.g.* when evaluating tails in the jet energy reconstruction or in the $E_{\mathrm{T}}^{\mathrm{miss}}$ distribution.

The information is stored in the GEANT HITS banks through an automated procedure: different types of hits are pre-defined (calorimeter-type hits, tracker-type hits), where the user can store all the information needed to reproduce the detector response at the digitisation step. Hits are produced at tracking time and stored in their respective branch of the HITS bank, to be eventually stored on tape at the end of each event. This procedure is in most cases automatic, since the program, which takes care of retrieving the appropriate information from the GEANT common blocks, stores it with the right format in the relevant HITS bank.

The information collected in the HITS banks, although dependent on the geometry used by GEANT for event tracking, is nevertheless very general and does not contain any assumption on the detector readout structure. It normally consists of hit positions (for tracking detectors) and energy losses (for calorimeters), and it provides the basis for the simulation of the detector response, which takes place at the digitisation step. HITS banks can be added together in order to simulate event superposition or pile-up (see Section 2.3).

The contents of the HITS banks are the most valuable output of the detector simulation program, since most of the CPU time used goes into producing them. The format of these banks (and the geometry description which has been used to produce them and which defines inherently their structure) must be kept as stable as possible. This is especially true for the case of event superposition or pile-up, in which the simulation of the minimum-bias events is particularly demanding in terms of CPU, and where consistency at the level of the HITS banks and of the geometrical description must be guaranteed. Table 2-2 shows a few examples of the CPU time needed to simulate particles or complete events through the ATLAS geometry. The CPU time needed for any physics event is essentially proportional to the amount of energy entering the calorimeters, where most of the CPU time is spent.

Table 2-2 CPU time needed for simulation of the ATLAS detector with GEANT 3.21. The timings, given in SPECint95 seconds for single tracks and for minimum-bias events, were obtained from the CPU time on a Pentium II processor at 400 MHz and scaled by the estimated SPECint95 rating of 10.3.

Event type	Timing in Inner Detector	Timing in Calorimeters
Single track (electron of 10 GeV energy)	6	100
Single track (pion of 10 GeV energy)	4	60
Minimum-bias event ($\|\eta\| < 3.0$)	190	2500

2.2.7 Digitisation

The digitisation step is a second level of detector simulation, placed just at the interface with the reconstruction program, where the physical information registered within the HITS bank is collected, re-processed in order to simulate the detector output, and eventually written out (in the GEANT DIGI structure) to be then used by the reconstruction programs. The output from the digitisation is obtained in a form similar to that which might be expected from the readout electronics in the actual experiment.

This step was in fact originally conceived to give the user the possibility of changing the readout characteristics (for instance, the strip pitch in the silicon detectors or the cell granularity in the EM Calorimeter) immediately after the detector simulation step, thus gaining considerably in the amount of CPU time needed during the phase of detector optimisation. Detailed signal treatment (for instance, the most accurate possible treatment of *dE/dx* in the TRT or digital filtering in the calorimeters), simulation of the front-end electronics behaviour, noise injection, *etc.*, can also be performed at this level.

The digitisation step is very fast, except when pile-up at high luminosity is included. It is often therefore rerun as the first step in the reconstruction chain, if noise levels or single-channel efficiencies in some of the detectors are to be varied.

2.3 Simulation of pile-up and radiation backgrounds

2.3.1 General considerations

The cross-section for inelastic, non-diffractive *pp* interactions at the LHC is ~70 mb. At the design luminosity of $10^{34}\,cm^{-2}s^{-1}$ and with a bunch spacing of 25 ns, the mean number of minimum-bias events which should be seen by the detector is 18. However, since approximately 20% of the buckets in the LHC will be empty, the average time between filled buckets is increased and the mean number of collisions is about 23 for these non-empty buckets. This implies that, when an interesting event is selected by the trigger, on average there will be 23 single minimum-bias events superimposed: these events are referred to as pile-up.

The bunch structure in LHC is such that there will be many successive filled buckets followed by successive empty buckets. This means that an interesting event will usually follow and be followed by beam-crossings containing pile-up events. Consequently, there is the potential for collisions from previous and following beam-crossings to be recorded by the detector, and this depends critically on the speed of response of the individual subdetectors.

The simulation of pile-up is normally performed just before and during the digitisation step: HITS banks from two different data streams (signal events and minimum-bias events), which have been simulated separately, are brought together, merged and then digitised. The number of minimum-bias events added to one single signal event is generated, beam-crossing per beam- crossing, based on a Poisson probability with a mean defined by the instantaneous luminosity of interest. Several beam-crossings surrounding the triggered beam-crossing can be generated with SLUG, so that the time structure of one complete event recorded by a particular detector can be faithfully reproduced. For those detectors with a signal collection time spanning over several beam-crossings, one can reproduce the time structure of one event; this feature, although very appealing, is not used in the standard pile-up simulation, since, for most of the simulated detectors, the time-of-flight information is not kept in the HITS banks.

A uniform method for simulating pile-up across all the detector systems has been used in general (the one exception is the Muon System, for which, as discussed in Section 2.3.4, the backgrounds are not correlated in time with the beam-crossing of interest). This method adds to each system, depending on its signal-collection speed, an equivalent average number of in-time beam-crossings, which would correctly simulate to first-order the real pile-up in the detector. For the pixel and SCT detectors, with their fast signal-processing speed, the equivalent number of pile-up events added on average is 24 (a multiple of 8 for technical reasons), for the slower TRT detector, with its 40 ns maximum drift-time, the equivalent number is 32 (which increases the straw hit occupancy by 30%) and finally, for all the calorimeter systems, the equivalent number is 48 (*e.g.* the EM Calorimeter has a 400 ns long drift time).

For most studies reported in the following chapters, this standard method for simulating pile-up has been applied by default. There are two notable exceptions to this:

- studies of fake rates in the TRT (see Section 3.5.3.2), using the full time-of-flight information for several beam-crossings around the trigger one, as described in Section 2.3.2;
- studies of pile-up effects in the calorimeter (see Section 4.3.2), using the exact pulse shape (together with optimal filtering at low luminosity) over five beam-crossings, as described in Section 2.3.3.

Since the effects from pile-up are the main concern for the survival and overall performance of the Inner Detector, it is important to note that:

- most of the hits seen in the Inner Detector arise from secondaries and not from the primary particles. In particular, the occupancies in the silicon sensors and the straws contain a significant contribution of 15 to 20% from primary particles produced at $|\eta| > 3.2$ and interacting with the beam pipe. On the other hand, the occupancies due to low-energy neutrons or photons are small with respect to the overall occupancy (see [2-2] for details).
- backsplash from particle showers initiating at or near the front face of the EM Calorimeter produces only a very small contribution to the occupancies in the Inner Detector. The predictions of GEANT 3.21 have been shown to under-estimate backsplash effects by as much as a factor of two [2-3];
- finally, the chosen threshold of 100 keV for most processes results in an under-estimate of the occupancies by about 10-15% (this has been demonstrated in test-beam measurements).

2.3.2 Pile-up in the TRT

In the Inner Detector, low-p_T tracks ($p_T < 400$ MeV) from beam-crossings prior to the one of interest will spiral in the solenoidal magnetic field for extended periods of time (up to 100 ns) and will therefore produce hits in the detectors over that period of time. In the TRT, the maximum drift time is around 40 ns, which is significantly more than the 25 ns bunch spacing, and the requirement to be as efficient as possible for in-time hits necessitates a gate which accepts some hits from fast particles from out-of-time events as well as hits from loopers.

As described above, the standard simulation of pile-up for the TRT superimposes 32 minimum-bias events, to allow for the extra hits which are expected from out-of-time beam-crossings. In reality, when reconstructed with the assumption that they were in time, these hits would be staggered about the true track positions to the left and right, depending on the drift direction in the straws. Instead, the standard simulation superimposes all the tracks in the TRT from a number of additional minimum bias events. These TRT hits are added in-time, hence they are explicitly correlated (*i.e.* they will really look like tracks in the TRT). It has been checked, using the complete simulation described below, that this creates a more difficult environment for pattern recognition than would be seen in reality (see Section 3.5.3).

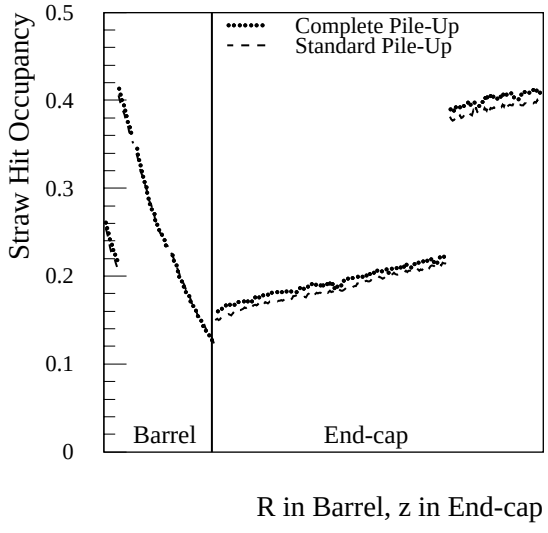

Figure 2-1 TRT straw hit occupancy at high luminosity using the complete time-of-flight method (dotted) and the standard method of adding hits from a total of 32 minimum bias events (dashed). The horizontal axis corresponds to layer number: in the barrel, this corresponds to radius; in the end-cap, this corresponds to *z*.

To understand these issues in detail, a more complete simulation has been performed for the TRT, which does describe correctly the time-structure of beam-crossings, particle and electrical propagation times, and allows parti-

cles to loop in the detector for as long as 250 ns. The results of these detailed simulations are described in [2-2]. It is from such studies that the effective number of events to be superimposed in the TRT for the standard simulation was determined. By design, the number of hits added is intended to ensure that the straw hit occupancy (a measure of the number of hits accepted by the gate associated with the LVL1 trigger and applied to the electronics) is the same as would be seen if the full timing information were used. At high luminosity, a mean of 24 minimum-bias events are expected to be in-time with the signal event. To these, a further eight events are added in the TRT to represent the out-of-time hits.

Figure 2-1 shows the straw hit occupancy using the full time-of-flight information and compares the occupancies with those from the standard method. As intended, the standard method provides a very good description of the occupancy and has the considerable advantage that the simulation code runs an order of magnitude faster.

2.3.3 Pile-up in the calorimeters

As discussed in Section 2.3.1, 23 minimum bias events (around 3500 particles over $|\eta| < 5.0$) are produced on average at each bunch crossing during high-luminosity operation. To cope with this environment, the ATLAS liquid-argon Calorimeters are read out using fast bipolar shapers with a peaking time of ~35 ns.

The standard pile-up simulation [2-4] assumes an average effective number of 48 minimum bias events, computed, for a typical signal shape, so as to obtain the same noise as if all the events were summed with the correct weighting. The advantages of this method are its simplicity and low CPU load, but it does not take into account the bipolar shaping (the pile-up energy distribution is not correct) and it is unable to provide multiple-sampling information.

A complete simulation program [2-5] has been now implemented. It takes into account the exact pulse shape, which depends on three time constants: the drift time, the shaper time constant, and an additional pole given by the gap capacitance and the preamplifier input impedance. Calorimeter data from fully-simulated minimum-bias events are weighted according to the shaper response of each type of cell. At high luminosity, about 700 minimum-bias events are needed to simulate one pile-up event. If required, five consecutive samples are computed in this way and stored separately. In this case, the electronic noise with the correct time correlations may also be superimposed. The digital filtering procedure may also be used. In this way, the electronic shaping is modified (within limits) to reduce the electronic noise when running at low luminosity.

As stated above, this much more accurate method of pile-up simulation will produce the correct spectra of transverse energies per cell from pile-up at high luminosity. In particular, the mean will be centred at zero, which is not the case for the standard simulation. However, as discussed in Section 4.2.4, the rms spreads of the pile-up energies obtained with both methods are very similar, leading to the conclusion that, for most effects, the difference between the two methods is very small.

2.3.4 Backgrounds in the Muon System

The physics performance of the ATLAS Muon System depends strongly on the level of background recorded in the active elements. The main source of this background is from particles produced in the interactions of primary hadrons from proton-proton collisions with the materi-

al of the detector (especially the calorimeters and the toroid structures), and with machine elements such as the collimators and the beam pipe. This background cannot be generated by the standard pile-up method described in Section 2.3.1.

The particles are neutrons, low-energy photons originating from neutron capture, and charged particles. The neutrons mostly have thermal energies, while the photons are concentrated in the 200 keV to 2 MeV energy range. The interaction of these photons with the detector material (aluminium in the case of the precision chambers, bakelite or G10 in the case of the trigger detectors) produces a signal in the sensitive volume of the chamber via the Compton effect with a probability of about 10^{-2}. Neutrons have a much lower probability to produce a direct signal in the muon detectors, but are directly responsible for the photon flux. The charged-particle background consists mainly of muons, charged pions, protons, electrons and positrons. The muons and pions are produced mostly in K^0 decays, while the protons emerge from neutron spallation processes. Hadrons and muons have a typical momentum of 100 MeV.

Detailed studies have been performed and reported in [2-6], using two Monte Carlo packages:

- GCALOR, which designates the CALOR package interfaced to GEANT. This package unfortunately does not contain many of the physics processes necessary to accurately estimate the backgrounds in the Muon System;
- FLUKA [2-7], which is the most developed package in terms of the implemented physics processes of relevance, but which cannot be interfaced readily to the detailed description of the detector geometry.

In practice, the standard ATLAS detector simulation package, based on GEANT, cannot simulate adequately the backgrounds from low-energy neutrons, photons and charged particles expected in the Muon System, because none of the GEANT-based packages provides adequate particle propagation at such low energies. Hence, other specialised programs, such as FLUKA, are used to simulate these backgrounds.

The muon-detector counting rate, as predicted by FLUKA, depends strongly on the muon station position and pseudorapidity. Typically, in the barrel chambers at high luminosity, the nominal rate in the first station is ~10 Hz/cm^2, and increases to 100 Hz/cm^2 around $|\eta| = 0.7$ (where the Tile Calorimeter gaps are located). For the end-cap chambers, the counting rate in the inner stations increases up to ~1 kHz/cm^2. The counting rate in all the other stations is significantly lower, with values in the range between 10 and 30 Hz/cm^2, and depends weakly on pseudorapidity. The dominant contribution to this rate comes from the photon flux, whereas charged particles contribute a rate of only a few Hz/cm^2.

The background studies are performed by conservatively multiplying the nominal Monte Carlo counting rates by a factor of ten, to evaluate the maximum expected counting rates in the Muon System. This large factor is justified by:

- the simplified implementation in FLUKA of the detector and shielding geometry (cracks which will inevitably appear in the real detector have not been taken into account);
- the difference between the effective nuclear composition of the materials which will be used in the experiment and that of the materials considered at present in the simulation;
- the uncertainties on the properties of the minimum-bias events (cross-section, particle composition, particle spectra, *etc.*);
- the uncertainties on particle transport and on the estimates of the sensitivity of the detectors to low-energy photons and neutrons.

The most important consequences of this background are:

1. high occupancy of the muon detectors, especially in the inner stations at large $|\eta|$;
2. space-charge effects;
3. reduced lifetime of the muon detectors;
4. high fake LVL1 muon trigger rate.

The first three effects are determined mainly by the intensity of the photon flux, and therefore indirectly by the intensity of the neutron flux. Muon track reconstruction studies [2-6] have shown that the physics performance of the Muon System begins to be degraded if the background level becomes larger than ten times the one presently estimated. Hence, it is very important to keep under constant control all changes proposed for the shielding system and the detector (*e.g.* the Tile Calorimeter gaps).

In contrast to the above, the most critical background for the LVL1 muon trigger rate is that from charged particles with a momentum around 100 MeV. With the design described in [2-8], the LVL1 muon trigger can only tolerate the nominal background rates, leaving almost no contingency for the uncertainties in the Monte Carlo predictions. Nevertheless, as discussed already to a certain extent in [2-8], improvements have been made to the trigger design to make it more robust against this type of background. The revised design and expected performance are documented in [2-9] (see also Section 11.3.1.6).

In order to allow physics simulation studies accounting for the background in the Muon System, a program that parametrises the particle rates and kinematics, as predicted by FLUKA in the region of the muon detectors, has been implemented. This program operates in the detector-simulation framework to digitise the hits collected in the muon detector in the same way as for physics events. At present, for the charged-particle backgrounds, only muons and pions have been simulated (within a simple model tuned to the FLUKA results). Concerning the simulation of the hits induced by photons (the neutron hit rate is negligible and therefore this source has been ignored), the only practical solution was to ‘inject’ directly, into the sensitive regions of the Muon System, Compton electrons with an energy close to the one predicted on average by FLUKA.

2.4 Reconstruction

The reconstruction of particles and other physics objects in the ATLAS detector has been developed over many years, and is implemented in a single program named ATRECON, based on the SLUG framework (see Section 2.2.2). ATRECON is mostly written in Fortran77, using ZEBRA as memory manager, although some parts have already been rewritten in C++, but not with a fully object-oriented design. This software will be replaced over the coming years by new OO software [2-10], which will use the existing software and its performance as a reference benchmark and will build from the algorithms and experience gained in developing ATRECON. ATRECON runs on fully simulated GEANT 3.21 data and does not handle raw data nor calibration / alignment constants. However, it is today rather complete, and can reconstruct full events with all detectors included, without using generator-level Monte Carlo information, in an acceptable amount of CPU time (see below).

The reconstruction proceeds in two stages (in addition to initialisation). First, data from each detector is reconstructed in a stand-alone mode. Second, the information from all detectors is combined to get the most accurate measurements and identification of the final objects used in the analysis: photons, electrons, muons, τ-leptons, K_S^0, jets, *b*-jets, E_T^{miss}, primary vertex, *etc*. This is described in great detail throughout this volume, and only a very brief summary is given below. The output of the various algorithms is stored in standardised ZEBRA banks, but control n-tuples and histograms are also available. The output is also stored in a menu-driven combined n-tuple, which allows rapid checks, analysis in a PAW framework and comparisons between algorithms. A third stage which is not described here, but rather in Chapters 14 to 21, is the analysis-specific part: reconstruction of exclusive *B* decays, *W*'s, *Z*'s, top quark decays, Higgs bosons, SUSY particles, *etc*. Figures 2-i and 2-ii show two views of a high-p_T reconstructed $H \rightarrow ZZ^* \rightarrow ee\mu\mu$ decay, with reconstructed tracks in the Inner Detector and the Muon System and with the reconstructed energy clusters of the two electrons and the high-p_T jet in the calorimeters.

2.4.1 Initialisation

At the start of reconstruction, the ATLAS geometry is rebuilt either from the event geometry as stored in ZEBRA banks from the simulation program, or from the ATLAS geometry database (AMDB). GEANT or AMDB routines are used during reconstruction to obtain the global coordinates of hits and cells. The magnetic field map is loaded. By default, the field is constant in the Inner Detector and as realistic as possible elsewhere, but some studies have been done with a realistic solenoidal magnetic field in the Inner Detector (see Section 3.5.4). Loading of calibration and alignment constants has not been implemented, except in an *ad hoc* way for some specific studies. The program is driven by datacards which allow a large spectrum of running conditions: switching on / off packages, changing noise levels, thresholds, efficiencies or internal algorithm parameters.

2.4.2 Stand-alone reconstruction

Matrices containing the energies in all calorimeter cells are filled. Jets are built following various algorithms with the cone algorithm used as a default (see Section 9.1). The E_T^{miss} vector is computed from the vector sum of the cell transverse energies (see Section 9.2).

Electromagnetic clusters are reconstructed in the barrel and end-cap EM Calorimeters (see Section 4.2.3). Modulations in the measurement of the positions and the energies, due to the finite cell / cluster sizes or to the detector geometry, are corrected for by using the known correlations between shower position and biases in position and energy. Standalone electron / gamma identification is performed using shower-shape variables.

Muon track segments in the Muon System are found from a combinatorial search of the single-station track segments, followed by a fit using the hits (see Section 6.3.1). The tracking, performed in the highly non-homogeneous magnetic field, takes into account multiple scattering in the material of the apparatus. The output is a list of tracks with parameters extrapolated back to the interaction region, and also a list of track segments in the inner stations, possibly corresponding to low-p_T muons, which cannot be reconstructed with high efficiency in a standalone mode.

Hit coordinates are reconstructed in the precision tracker and in the TRT. Tracks from charged particles are searched for (see Section 3.1.2). Three rather different algorithms with comparable performances have been developed:

- iPatRec starts from a combinatorial search in the precision tracker;
- PixlRec uses a track-following algorithm starting from the pixel *B*-layer outwards;
- xKalman finds tracks in the TRT with a histograming method and follows them inwards using Kalman-filtering techniques.

Track reconstruction can be performed over the full Inner Detector (except for iPatRec), or over a limited $\Delta\eta\times\Delta\phi$ range around 'seeds' found by the other detectors (electromagnetic clusters, jets, muons) and around Monte-Carlo truth information for checks. Seeds cannot be used for events like inclusive *b* production ($b\overline{b}\rightarrow\mu_6 X$, *i.e.* events containing a muon with $p_T > 6$ GeV), where all tracks need to be reconstructed. The use of seeds in the reconstruction algorithm can save a factor of up to 100 in CPU time for events including the pile-up expected at high luminosity.

Trigger algorithms have so far been developed in an independent package (see Chapter 11), but it is possible to run LVL1 and LVL2 trigger algorithms prior to reconstruction.

2.4.3 Combined reconstruction

In a second stage, information from several detectors is combined. Muons reconstructed in the Muon System are refined by matching the track to an Inner Detector track (see Section 8.1). This improves the momentum resolution, especially at moderate p_T, and yields accurate track parameters at the vertex. Lower-p_T (down to 2 GeV) muons are found by matching an Inner Detector track to the Tile Calorimeter cells (see Sections 8.2 and 10.4.2).

Photon conversions (see Section 7.5.1) and K_S^0 decays (see Section 3.6.2.1) are searched for by pairing Inner Detector tracks. The primary vertex is reconstructed using all the tracks in the event (see Section 3.6.1).

High-p_T (above 10 GeV) photon identification requires electromagnetic cluster shower-shape variables and the absence of reconstructed tracks in the Inner Detector, except for identified conversions (see Sections 7.5 and 7.7). High-p_T electron identification requires a track reconstructed in the Inner Detector with transition-radiation hits and a measured momentum matching a calorimeter energy deposition compatible with an electromagnetic shower (see Section 7.4). Softer non-isolated electrons (down to p_T of 1 GeV) are identified by extrapolating Inner Detector tracks to the EM Calorimeter (see Section 7.3.1).

Finally, τ-leptons are identified from narrow jets associated with a small number of charged tracks (see Section 9.1.5). Candidate *b*-jets are tagged by combining the impact parameter of high-quality tracks with soft electrons or muons (see Chapter 10).

2.4.4 Timing

The complete reconstruction is seldom needed for any particular analysis. The various items are split into different packages that can be activated or not to save CPU time. Even though reconstruction speed has always been a concern, the algorithms have been tuned to obtain the best

possible performance (efficiency and resolution) rather than the fastest execution time. Significant improvements are still possible for all packages. Table 2-3 shows, as an illustration, the present average CPU time needed to reconstruct different types of events. There is a significant degradation in speed of all algorithms at high luminosity, although some of it can be recovered in the Inner Detector by using seeds. Even low-luminosity pile-up increases significantly the time needed for track reconstruction. In practice, the CPU time needed depends significantly on parameters like the size of the $\Delta\eta\times\Delta\phi$ window (here 0.1×0.1 for single tracks, 0.5×0.5 for jets), the minimum p_T to be reconstructed (1 GeV in the example shown below), the cell energy thresholds and internal parameters. The timing for muon reconstruction scales with the number of muons and is relatively independent of luminosity. It does however depend on the muon p_T with an optimum around 50 GeV and a degradation of more than a factor of two at low p_T (low-momentum tracking in the highly inhomogeneous field) and at high p_T (handling of electromagnetic showers).

Table 2-3 Timing obtained for the most important reconstruction packages for some typical events in SPECint95 seconds. No minimum-bias events were added for the generic studies, 2.3 were added for low-luminosity operation and 23 for high-luminosity operation. The timings are quoted for PA8000 processors at 180 MHz, scaled by the estimated SPECint95 rating of 7.

Event	Muon	Calorimeter	xKalman (complete events)	xKalman (seed)	iPatRec (seed)
$b\bar{b} \rightarrow \mu_6 X$	238	9	26	-	-
$b\bar{b} \rightarrow \mu_6 X$ at low luminosity	238	9	99	-	-
$WH \rightarrow \mu\nu b\bar{b}$ with m_H = 100 GeV	154	12	39	26	9
$WH \rightarrow \mu\nu b\bar{b}$ with m_H = 100 GeV at high luminosity	170	93	2660	366	40
$H \rightarrow ZZ^* \rightarrow ee\mu\mu$ with m_H = 130 GeV	242	10	24	7	4

2.5 Fast simulation and reconstruction

Fast particle-level simulation and reconstruction is an intermediate step between simple parton-level analysis of the event topology, which in general yields much too optimistic results for physics processes at hadron colliders, and very sophisticated and CPU-consuming full detector simulation (see Section 2.2) and reconstruction (see Section 2.4). This kind of approach is needed for quick and approximate estimates of signal and background rates for specific channels. In addition, fast simulation and reconstruction is the only practical tool for high-statistics studies of complex background processes.

A complete package for fast detector simulation and physics analysis has been implemented over the past few years and exists in two implementations:

- ATLFAST, the FORTRAN implementation of the algorithm [2-11], interfaced to PAW;
- ATLFAST++, the OO/C++ implementation of the same algorithm [2-12], interfaced to ROOT [2-13].

Both versions have been used for the results presented in this document.

ATLFAST can be used for fast simulation of signal and background processes, including the most crucial detector aspects: jet reconstruction in the calorimeters, momentum/energy smearing for leptons and photons, magnetic field effects and missing transverse energy. It provides, starting from the list of particles in the event, a list of reconstructed jets, isolated leptons and photons, the expected missing transverse energy, and reconstructed charged tracks. Values for the rejections against non-*b* jets and non-τ jets are also provided as a function of the efficiencies for identifying *b*-jets and τ-jets. In most cases, the detector-dependent parameters are tuned to what is expected for the performance of the ATLAS detector from full simulation and reconstruction (see below).

The ATLFAST package aims to reproduce as well as possible the expected detector performance in terms of resolution and particle-identification for important physics signals. It does not attempt, at present, to reproduce accurately the expected efficiencies for lepton and photon isolation. In the case of hadronic jets, the jet reconstruction (and veto) efficiency is often dominated by physics effects, which are straightforward to model in the fast simulation. For any specific channel, the predictions from ATLFAST in terms of resolution and reconstruction efficiency, should always be confirmed with full-simulation results. Such detailed comparisons have been done in many cases, *e.g.* for the WH, $H \rightarrow b\bar{b}$ [2-14], $H/A \rightarrow \tau\tau$ [2-14] and $H \rightarrow WW \rightarrow l\nu jj$ [2-15] channels, as well as for several Higgs-boson decay channels with multi-*b*-jet final states [2-16]. The acceptances, jet reconstruction efficiencies, jet-veto efficiencies, and mass resolutions have shown good agreement between fast and full simulations.

Not all the detector effects can be readily parametrised in fast simulation and only the basic information of the detector geometry is used in the package. This basic information is for example: the η-coverage for precision physics and for the calorimetry, the size of the barrel/end-cap transition region for the EM Calorimeter, and the granularity of the hadronic calorimeters. No effects related to the detailed shapes of particle showers in the calorimeters, the charged track multiplicity in jets, *etc.*, are taken into account. In particular, energy isolation of leptons is only simulated in a crude way.

For practical reasons, the package has been divided into two parts: the main ATLFAST package, executed on the generated events, and a supplementary package, ATLFAST-B, which can be executed on the filtered n-tuples during user analysis. In the following, the main features of ATLFAST and their relationship to the full simulation and reconstruction results are described.

2.5.1 Calorimeter clusters

The transverse energies of all undecayed particles, except for neutrinos, muons and the SUSY *LSP*, are summed up in calorimeter cells of granularity 0.1x0.1 over $|\eta| < 3.2$, and 0.2x0.2 (for $|\eta| > 3.2$) in $\eta \times \phi$ coordinates over the full calorimeter coverage. The effect of the solenoidal 2 T magnetic field on the ϕ-position of charged particles with p_T above 0.5 GeV threshold is parametrised. It has been checked that the contribution from charged particles with p_T below this threshold can be neglected. A fixed-cone algorithm is used for the cluster reconstruction (see Table 2-4 for the expected efficiencies of cluster reconstruction); other reconstruction algorithms can be also activated as options.

Table 2-4 Efficiency for cluster reconstruction at low luminosity, for different types of initial partons with $p_T^{parton} > 15$ GeV and $p_T^{jet} > 15$ GeV.

Type of initial parton	Reconstruction efficiency in $\Delta R < 0.4$
u-quark	83%
b-quark	76%
gluon	74%

2.5.2 Isolated electrons and photons

Photon and electron candidates, isolated from any hadronic activity, are searched for in the particle list. The polar angle of the photon and the photon and electron four momenta are smeared with a parametrisation directly derived from the full simulation. Isolation criteria in terms of distance from other clusters and of maximum transverse energy deposition in a cone around the photon / electron candidate, as well as the geometrical acceptance, are verified. As a benchmark, the resolutions expected for $H \to \gamma\gamma$ and $H \to ZZ^* \to 4e$ reconstruction show reasonable agreement between the parametrisation used for the fast simulation and the expected performance from full simulation, as shown in Table 2-5.

Table 2-5 Expected mass resolutions for a few benchmark processes, as obtained from fast and full simulation.

Process	ATLFAST	ATLAS
$H \to \gamma\gamma$, $m_H = 100$ GeV	$\sigma_m = 1.2$ GeV (high L)	$\sigma_m = 1.3$ GeV (high L)
$H \to ZZ^* \to 4e$ $m_H = 130$ GeV	$\sigma_m = 1.6$ GeV (high L)	$\sigma_m = 1.8$ GeV (high L)
$H \to ZZ^* \to 4\mu$ $m_H = 130$ GeV	$\sigma_m = 1.3$ GeV (combined ID+ Muon System)	$\sigma_m = 1.4$ GeV (combined ID+ Muon System)

2.5.3 Isolated muons

Isolated muon candidates are searched for in the particle list. Each muon momentum is smeared according to a resolution parametrised as a function of muon p_T, $|\eta|$ and ϕ. Three options depending on which subdetectors are assumed to be used for the muon measurement can be invoked: Muon System stand-alone, Inner Detector stand-alone (parametrisation from [2-17]) and combined Inner Detector plus Muon System. Isolation criteria in terms of distance from other clusters and of maximum transverse energy deposition in a cone around the muon candidate, as well as the fiducial geometrical acceptance, are applied. As a benchmark, the mass resolution expected for the $H \to ZZ^* \to 4\mu$ reconstruction shows reasonable agreement between the parametrisation used for the fast simulation and the expected performance from full simulation (see Table 2-5).

ATLFAST does not correct for efficiencies in the reconstruction / identification of muons, electrons nor photons, so the estimated efficiencies (from the full simulation study) should be included by the user in the event analysis. However, the package simulates muon trigger efficiencies if required to, and isolated and non-isolated muons are flagged with an appropriate flag.

2.5.4 Jets and pile-up

Clustered cells are used for the jet reconstruction. As a default, a cone size of 0.4 is used. The energies of clusters, which have not been selected as associated with isolated electrons or photons, are smeared with the energy resolution, parametrised according to results from full simulation of the hadron calorimeters [2-4]. Two options can be invoked: low luminosity and high luminosity. In the latter case, the expected effects from pile-up are included in the parametrisation of the resolution. The measured momenta from non-isolated muons which fall inside the cluster cone and are within $|\eta| < 2.5$ is added to the smeared cluster energy. Reconstruction with the JetFinder library [2-18] of alternative jet algorithms is also implemented.

Table 2-6 Reconstructed mass peak position and rms width for generated *WH* events with m_H = 100 GeV.

Final state	$\langle m_{jj} \rangle$ (GeV)	σ_m (Gev)	Acceptance in $m_H \pm$ 20 GeV
$H \to b\bar{b}$	103.0	12.5	90%
$H \to u\bar{u}$	100.7	8.2	86%
$H \to gg$	101.3	11	79%

2.5.5 Jet energy recalibration

The effect of the energy loss outside the cone is corrected using a p_T^{jet}-dependent calibration factor, calculated as an average p_T^{parton} / p_T^{jet}. The set of calibration factors, separately for *b*-jets and light-quark jets, is provided in the supplementary package ATLFAST-B. Table 2-6 shows the expected mass resolution, acceptance and peak position for the *WH* process. This calibration is process independent, however it might be optimised depending on the average p_T of the initiating partons.

Table 2-7 Mass resolution and acceptance for reconstructed *WH* decays with $H \to b\bar{b}$, using standard recalibration and clustering algorithm.

m_H = 400 GeV	σ_m (GeV)	Acceptance in $m_H \pm 2\sigma_m$
Standard recalibration	52	82%
Clustered jets	45	77%

In some cases, for the reconstruction of high-mass resonances, a better procedure is to collect into a cluster the jets reconstructed inside a larger cone, *e.g.* ΔR = 0.8, and applying recalibration to clustered jets only. Table 2-7 compares the resolutions and acceptances obtained for $H \to b\bar{b}$ reconstruction with m_H = 400 GeV (the intrinsic Higgs width was set to zero for this comparison).

2.5.6 *b*-tagging

Of special interest are jets originating from *b*-quarks (so-called *b*-jets) which can be identified using *b*-tagging techniques (vertex or soft-lepton tags). The package labels a jet as a *b*-jet, if a *b*-quark of $p_T > 5$ GeV (after final-state radiation) is found in a cone of $\Delta R = 0.2$ around the reconstructed jet for jets with $|\eta| < 2.5$. These criteria have been discussed in more detail in [2-2]. Jets originating from *c*-quarks are labelled as *c*-jets if similar criteria are satisfied.

Table 2-8 Assumed nominal performance for *b*-tagging of *b*-labelled jets at low and high luminosity

Efficiency	Low luminosity	High luminosity
ε_b	60%	50%
ε_c	10%	10%
ε_j	1%	1%

ATLFAST does not include efficiencies for *b*-jet tagging or non-*b* jet rejection. In the supplementary package ATLFAST-B, for *b*-labelled jets, efficiencies for tagging and inefficiencies for mistagging *c*-jets and other jets have been parametrised as p_T-dependent functions. These parametrisations can be applied randomly by the user during event analysis (Table 2-8 shows the nominal parametrisation averaged over p_T). Detailed comparisons between these parametrisations and results from *b*-tagging algorithms for the fully simulated events, as presented in Chapter 10, can also be found in [2-11].

2.5.7 τ-tagging and τ-veto

Jets originating from τ-decay (so-called τ-jets), can be identified in the case of hadronic τ–decays. A systematic study of the ATLAS potential for τ identification has been documented in [2-19] (see also Section 9.1.5). In the case of fast simulation, τ-jet candidates are τ-labelled if the hadronic τ-decay product(s) is relatively hard (default: $p_T^{\tau\text{-}had} > 10$ GeV), inside tracking range ($|\eta| < 2.5$), dominates reconstructed jet (default: $p_T^{\tau\text{-}had}/p_T^{\text{jet}} > 0.9$) and within jet cone (default: $\Delta R_{\text{jet},\,\tau\text{-}had} < 0.3$). These criteria are consistent with the identification procedure of fully simulated events. The efficiency for τ-labelling is 92% for τ-hadronic decays from $A \rightarrow \tau\tau$ and for $m_A = 300$ GeV.

A τ-veto can be useful for the rejection of backgrounds containing τ-leptons. A more detailed study of the τ-veto was done using $A \rightarrow \tau\tau$ events and a large sample of jet events, as presented in [2-19], using cut-offs on the electromagnetic radius and on the number of associated tracks with $p_T^{\text{track}} > 1$ GeV. As an example, for $p_T^{\text{cluster}} > 60$ GeV, $\varepsilon^{\text{veto,jet}} = 90\%$ with $\varepsilon^{\text{veto},\tau} = 5\%$ can be achieved.

ATLFAST does not correct for efficiencies for τ-jet identification or other jet misidentification. For τ-labelled jets, the efficiencies for τ tagging and mistagging have been parametrised [2-19] and are available in supplementary package ATLFAST-B.

2.5.8 Track reconstruction

The track reconstruction is provided for charged, stable particles inside the Inner Detector coverage. Reconstructed track parameters (d_0, b, ϕ, $\cot(\theta)$, q/p_T) are smeared with parametrisation from [2-17] as derived from the studies for the Inner Detector TDR [2-2]. Parametrisation for

muons, pions (including tails) and electrons (including bremsstrahlung) as well as the respective reconstruction efficiencies, are available. This implementation is dedicated mainly to the *B*-physics studies.

2.5.9 Missing transverse energy

The missing transverse energy, E_T^{miss}, is calculated by summing-up the transverse momenta of identified isolated photons, electrons and muons, jets, *b*-jets and *c*-jets, and of non-isolated muons not added to any jet cluster. Finally, the transverse energies deposited in cells not used for cluster reconstruction are also included in the total sum. Transverse energies deposited in unused cells are smeared with the same energy resolution function as for jets. In case of high luminosity, pile-up is included in the smearing parametrisation for energy deposited in unused cells. From the calculation of this total sum E_T^{obs} the missing transverse energy is obtained, $E_T^{miss} = E_T^{obs}$, as well as its components, $p_x^{miss} = -p_x^{obs}$, $p_y^{miss} = -p_y^{obs}$. The E_T^{miss} resolution given by ATLFAST for di-jet events with $p_T > 17$ GeV at low luminosity, $\sigma_{miss} = 5.7$ GeV, is consistent with what is expected from the full simulation of the ATLAS detector (see Section 9.1.5). Since ATLFAST is not adding pile-up to cells which remain empty after particle energy deposition, the high-luminosity result of $\sigma_{miss} = 11.3$ GeV represents an optimistic estimate.

2.5.10 Trigger selections

A primitive trigger routine to validate selected physics events can be invoked after each event has been analysed by the algorithm. This routine is not meant to cover the complete trigger menus, but rather to eliminate events which have essentially no chance of passing the LVL1 and LVL2 trigger as specified in the trigger menus today [2-20] (see also Section 11.7.3). It is more specifically dedicated to SUSY-particle searches, which will include many complex topologies of the type: n-jets + m-leptons + E_T^{miss}.

The proposed trigger selection is aimed at being compatible with the present LVL1/LVL2 understanding; slightly lower thresholds than in [2-20] are used for some cases where it might turn out to be justified from the physics and where it is not clearly impossible to implement. Three classes of trigger particles are used for low- and high-luminosity performance: isolated electrons and photons, muons and jets. For muons, a parametrised trigger efficiency, as studied in [2-6], is included. For electrons/photons and jets a trigger efficiency of 100% is assumed.

2.5.11 Mass reconstruction in multi-*b*-jet channels

To illustrate the consistency between fast and full simulation and reconstruction (see also Section 9.3) the mass reconstruction of the WH with $H \rightarrow b\bar{b}$ process with $m_H = 100$ GeV is presented in Figure 2-2. Jets with $p_T > 15$ GeV before energy recalibration are accepted and the efficiency for reconstruction is about 80% per *b*-jet from fast and full simulation. The mass peak can be reconstructed with an expected resolution of ~15 GeV with full simulation (resp. 12.5 GeV with fast simulation) and a correct position of the peak in the distribution (after jet energy recalibration), nevertheless with a some fraction of the signal appearing as non-Gaussian tails. Most of these effects can be attributed to the final-state radiation and hadronisation, as discussed in detail in [2-11]. More details on the comparison between full and fast simulation and reconstruc-

tion for multi-*b*-jet final states of Higgs-boson decays can be found in [2-16]. Some benchmark numbers, illustrating the good agreement between fast and full simulation, are collected in Table 2-9.

Table 2-9 Acceptances and resolutions for full and fast simulation of several Higgs-boson signatures in multi-*b*-jet channels for low-luminosity operation (the *b*-tagging efficiency is not included). When two resonances are present, the second one is reconstructed after applying a mass constraint on the first one.

Reconstructed events	*b*-jets	Resonance 1 σ_m (GeV)	Resonance 1 Acceptance in $\pm 2\sigma_m$	Resonance 2 σ_m (GeV)	Resonance 2 Acceptance in $\pm 2\sigma_m$
WH with $H \to b\bar{b}$ (see Section 19.2.4.2) (m_H = 100 GeV and p_T^{jet} > 15 GeV)	2 *b*-jets	$H \to b\bar{b}$	$H \to b\bar{b}$		
Full simulation	65%	14.7	89%		
Fast simulation	65%	12.5	90%		
WH with $H \to b\bar{b}$ (see Section 19.2.4.2) (m_H = 400 GeV and p_T^{jet} > 75 GeV)	2 *b*-jets	$H \to b\bar{b}$	$H \to b\bar{b}$		
Full simulation	72%	45	84%		
Fast simulation	71%	40	73%		
$A \to Zh \to llb\bar{b}$ (see Section 19.3.2.10) (with m_A = 300 GeV)	2 *b*-jets	$h \to b\bar{b}$	$h \to b\bar{b}$	$A \to Zh$	$A \to Zh$
Full simulation	61%	11.2	80%	8.6	71%
Fast simulation	64%	10.1	82%	7.8	75%
$H \to hh \to b\bar{b}b\bar{b}$; ($m_H$ = 300 GeV and p_T^{jet} > 15 GeV)	4 *b*-jets	$h \to b\bar{b}$	$h \to b\bar{b}$	$H \to hh$	$H \to hh$
Full simulation	40%	9.2	89%	13.1	82%
Fast simulation	45%	8.7	87%	12.8	83%
$t\bar{t}H$ with $H \to b\bar{b}$ (see Section 19.2.4.3) (m_H = 100 GeV)	4 *b*-jets	$t \to jjb$	$t \to jjb$	$H \to b\bar{b}$	$H \to b\bar{b}$
Full simulation	25%	11.7	75%	20.0	66%
Fast simulation	32%	10.0	80%	19.0	65%
$t\bar{t}$ with single top reconstruction (p_T^{jet} > 40 GeV)	2 *b*-jets	$W \to jj$	$W \to jj$	$t \to jjb$	$t \to jjb$
Full simulation	37%	8.1	87%	13.4	83%
Fast simulation	43%	7.3	82%	11.4	78%

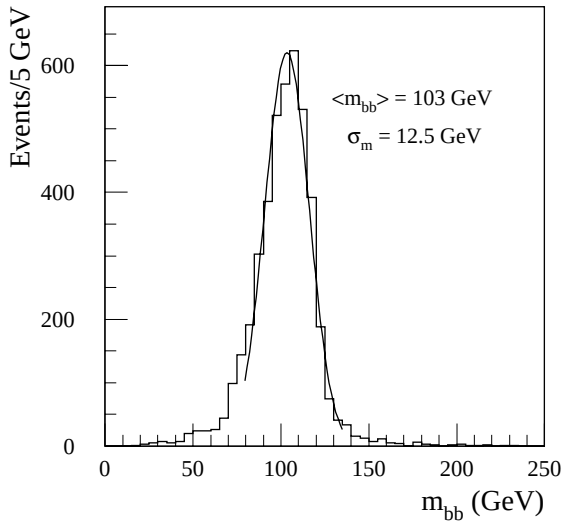

Figure 2-2 Distribution of reconstructed invariant mass, $m_{b\bar{b}}$, as obtained using fast simulation of *WH* production with m_H = 100 GeV and $H \rightarrow b\bar{b}$ decay at low-luminosity operation.

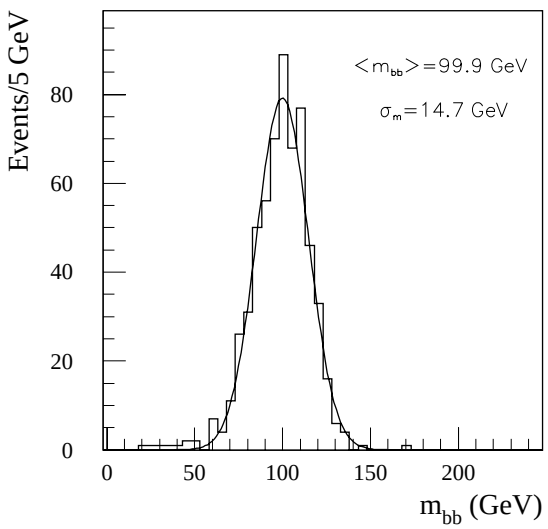

Figure 2-3 Same as Figure 2-2, but using full simulation of the ATLAS detector (see Section 9.3.2).

2.6 References

2-1 R. Brun *et al.*, GEANT3, CERN / DD / EE / 84-1 (1996).

2-2 ATLAS Collaboration, Inner Detector Technical Design Report Vol. I, ATLAS TDR 4, CERN / LHCC 97-16 (1997).

2-3 W. Funk, 'Study of backsplash effects in the TRD tracker', ATLAS Internal Note ATL-INDET-93-032 (1993).

2-4 ATLAS Collaboration, Calorimeter Performance Technical Design Report, ATLAS TDR 1 CERN / LHCC 96-40 (1996).

2-5 S. Simion, 'Pile-up simulation for ATLAS Calorimeters', ATLAS Internal Note ATL-SOFT-99-001 (1999).

2-6 ATLAS Collaboration, Muon Spectrometer Technical Design Report, ATLAS TDR 10, CERN / LHCC / 97-22 (1997).

2-7 A. Ferrari *et al.*, Z. Phys. **C70** (1996) 413; and FLUKA manual http: / / www.cern.ch / alice / Projects / offline / Simulation / fluka.

2-8 ATLAS Collaboration, First-Level Trigger Technical Design Report, ATLAS TDR 12, CERN / LHCC / 98-14 (1998).

2-9 Level-1 muon trigger group, 'Improvements to the level-1 muon trigger giving increased robustness against backgrounds', ATLAS Communication ATL-COM-DAQ-99-011 (1999).

2-10 ATLAS Collaboration Computing Technical Proposal, CERN / LHCC / 96-43 (1996).

2-11 E. Richter-Was, D. Froidevaux and L. Poggioli, 'ATLFAST 1.0 A package for particle-level analysis', ATLAS Internal Notes ATL-PHYS-96-079 (1996) and ATL-PHYS-98-131 (1998).

2-12 R. Brun and E. Richter-Was, 'Getting started with ATLFAST++', http://atlasinfo.cern.ch/Atlas/GROUPS/PHYSICS/HIGGS/ATLFAST-www/OOimplementation.html.

2-13 R. Brun et al., http://root.cern.ch.

2-14 D. Cavalli and S. Resconi, 'Comparison between full and fast simulation of ATLAS detector', ATLAS Internal Note ATL-PHYS-97-100 (1997).

2-15 P. Savard and G. Azuelos, 'The discovery potential of a Heavy Higgs (m_H = 800 GeV) using full GEANT simulation of ATLAS', ATLAS Communication ATL-COM-PHYS-98-007 (1998).

2-16 D. Cavalli and M. Sapinski, 'Full and fast simulation and reconstruction of Higgs decay channels with multi-b-jet final states', ATLAS Communication ATL-COM-PHYS-99-033 (1999).

2-17 E. J. Buis *et al.*, 'Parametrisation of the Inner Detector Performance', ATLAS Internal Note ATL-INDET-97-195 (1997); 'Update of Inner Detector Performance Parametrisation', ATLAS Internal Note ATL-INDET-98-215 (1998).

2-18 M. Bosman *et al.*, 'Jet Finder Library: version 1.0', ATLAS Internal Note ATL-SOFT-98-038 (1998).

2-19 D. Cavalli and S. Resconi, 'Tau-jet separation in ATLAS detector', ATLAS Internal Note ATL-PHYS-98-118 (1998).

2-20 ATLAS Collaboration, Trigger Performance Status Report, CERN/LHCC/98-15 (1998).